Please cite this article in press as: Vesga et al., Quantitative characterization of membrane-protein reversible association using FCS, Biophysical Journal (2023), https://doi.org/10.1016/j.bpj.2023.01.026

Biophysical Journal
Article

Biophysical Society

Quantitative characterization of membrane-protein reversible association using FCS

Arturo G. Vesga,[1,2] Lupe Villegas,[1] Cintia C. Vequi-Suplicy,[3] Carlos O. S. Sorzano,[1] and Jose Requejo-Isidro[1,2,*]
[1]Centro Nacional de Biotecnología (CNB), CSIC, 28049 Madrid, Spain; [2]Unidad de Nanobiotecnología, CNB-CSIC-IMDEA Nanociencia Associated Unit, 28049 Madrid, Spain; and [3]IMDEA Nanociencia. 28049 Madrid, Spain

ABSTRACT Functionally meaningful reversible protein-membrane interactions mediate many biological events. Fluorescence correlation spectroscopy (FCS) is increasingly used to quantitatively study the non-reversible binding of proteins to membranes using lipid vesicles in solution. However, the lack of a complete description of the phase and statistical equilibria in the case of reversible protein-membrane partitioning has hampered the application of FCS to quantify the partition coefficient (K_x). In this work, we further extend the theory that describes membrane-protein partitioning to account for spontaneous protein-membrane dissociation and reassociation to the same or a different lipid vesicle. We derive the probability distribution of proteins on lipid vesicles for reversible binding and demonstrate that FCS is a suitable technique for accurate K_x quantification of membrane-protein reversible association. We also establish the limits to K_x determination by FCS studying the Cramer-Rao bound on the variance of the retrieved parameters. We validate the mathematical formulation against reaction-diffusion simulations to study phase and statistical equilibria and compare the K_x obtained from a computational FCS titration experiment with the experimental ground truth. Finally, we demonstrate the application of our methodology studying the association of anti-HIV broadly neutralizing antibody (10E8-3R) to the membrane.

SIGNIFICANCE The reversible association of peptides and proteins with biological membranes is key to many cellular and physiological processes, as well as of growing interest for the pharmaceutical and biomedical industries. In this work, we tackle the quantification of protein-membrane affinity for proteins that spontaneously dissociate and reassociate from and to the membrane, taking into account how proteins distribute on lipid vesicles using fluorescence correlation spectroscopy (FCS). We further extend the methodological spectrum of available techniques to study membrane-mediated biological events, introducing a method that allows a most rigorous quantitative description of proteins that spontaneously dissociate and reassociate from and to the membrane.

INTRODUCTION

Reversible interaction of peptides and proteins with biological membranes is key to many cellular and physiological processes, such as signaling and antigen recognition, as well as of growing interest for the pharmaceutical and biomedical industries (1–3). The functional outcome of these interactions depends on protein partitioning between the aqueous buffer and the membrane. Due to the nature of lipid bilayers, membrane-protein interaction and, thus, protein partitioning to the membrane is dependent on the chemical species involved in the interaction but also on membrane collective properties such as viscosity and electrostatic surface potential (4,5). The quantitative study of the affinity of proteins for the membrane is crucial to unravel the mechanics of protein-membrane association, to understand the role of the membrane collective biophysical properties on the interaction (4), and to determine the energetics of protein-membrane association or protein insertion (6). An added complication to describe protein-membrane association is that, on most occasions, biomolecules associate to the membrane through a combination of several mechanisms: stoichiometric binding to one or several lipid molecules, adsorption to the bilayer through electrostatic attraction (non-stoichiometric interaction), or partial or complete insertion into the hydrophobic core of the lipid bilayer driven by the hydrophobic effect (7,8). For this reason, methodologies or models that presume a specific binding stoichiometry do not adequately describe the interaction. Instead, the partition coefficient allows

Submitted August 30, 2022, and accepted for publication January 20, 2023.
*Correspondence: jose.requejo@csic.es
Editor: Alberto Diaspro.
https://doi.org/10.1016/j.bpj.2023.01.026

Please cite this article in press as: Vesga et al., Quantitative characterization of membrane-protein reversible association using FCS, Biophysical Journal (2023), https://doi.org/10.1016/j.bpj.2023.01.026

quantification of the non-stoichiometric interaction of a molecule in aqueous solution with a biomembrane (6,9).

The partition coefficient (termed K_x or K_p) can be determined using a variety of methods, including centrifugation, calorimetry, and fluorescence spectroscopy (6,9,10). Most methodologies used to determine K_x rely on lipid molecules that self-assemble in the aqueous solution forming lipid vesicles. Upon association, proteins or peptides do not distribute evenly onto vesicles, but they follow a particular probability distribution so that every vesicle carries a different number of proteins. For this reason, in addition to phase equilibrium, the characterization of partitional behavior requires statistical equilibrium to be considered through the description of its probability distribution. It has been acknowledged that the description of the protein distribution on vesicles is critical to precise K_x determination, and the case of non-reversible binding has already been successfully addressed (11–13). However, to our knowledge, the effect of dissociation and reassociation events on the distribution of proteins on vesicles and, as a consequence, on K_x quantification has so far not been considered. Thus, quantitative understanding of partitional behavior is undermined by the lack of models that fully describe reversible association.

K_x determination is frequently performed using methods based on fluorescence spectroscopy (e.g., (10,14) and references therein). They are highly sensitive and, threfore, measurements can be performed at low solute concentrations. In addition, no physical separation of phases is required, resulting in minimal perturbation of the partition equilibrium (9). Fluorescence correlation spectroscopy (FCS) and fluorescence cross-correlation spectroscopy (FCCS) are highly sensitive spectroscopic techniques based on the analysis of the fluctuations of the emission of fluorescently tagged particles (e.g., molecules or lipid vesicles) as they traverse a very small detection volume (15,16). FCS is particularly suited to study binding and insertion of biomolecules into the membrane as it requires very low protein concentration and has single-molecule sensitivity (13,17–20). FCS is also advantageous as it allows molecules to be labeled at non-interfering locations away from the protein-membrane interaction site, thus avoiding potential perturbation of the partition equilibrium due to fluorophore-membrane interactions.

In this work, we tackle the quantification of protein-membrane affinity for proteins that spontaneously dissociate and reassociate from and to the membrane taking into account how proteins distribute on lipid vesicles in equilibrium. We extend and improve previous work that described the use of FCS for the case of non-reversible association (13,17–20) and demonstrate that FCS accurately determines the binding constants in the case of reversible association. To do so, we first derive the mathematical formulation of the probability distribution of proteins on vesicles and test it against an in silico reaction-diffusion experiment. We then study the application of this mathematical formulation to determine K_x using titration FCS experiments. We validate the use of this probability distribution using computational FCS and we study the Cramer-Rao bound (CRB) on the variance of the retrieved parameters to establish the accuracy and the application limits for the quantification of reversible association using FCS.

Finally, we demonstrate our work by quantifying protein-membrane reversible association for a highly relevant biotechnological application, namely the optimization of an anti-HIV-1 antibody (Ab) (10E8) by engineering its membrane avidity. 10E8 is capable of blocking infection by almost all HIV-1 strains (21), and it has recently been shown that the promotion of membrane interactions of the 10E8 broadly neutralizing Ab can significantly increase its potency without increasing its polyreactivity (22,23). Thus, accurate quantitative description of the interactions of the Ab and the viral membrane is paramount to the rational design of HIV-optimized Abs. In turn, this is of great interest to developing vaccines (24) and treating HIV infection by passive immunization (25).

THEORY

Here, we formulate the probability distribution of proteins that reversibly associate to lipid vesicles and establish the framework to quantify protein-membrane affinity in this case. All symbols used throughout the text are summarised in Table 1.

Phase equilibrium

Proteins at an aqueous/membrane interface undergo a continuous series of association and dissociation events at a rate that depends on the polar properties of the aqueous buffer, the membrane core and its interface, and the biomolecule itself. In phase equilibrium, the rates of protein association and dissociation to and from the lipid membrane are equal and the amount of membrane-bound protein fluctuates around a stationary value. Assuming that the accessible lipid concentration is sufficiently large, so that the membrane does not saturate with bound protein, the mole fraction partition coefficient can be defined as (6,9):

$$K_x = \frac{m^p_{mem}/m_L}{m^p_{aq}/m_W} \tag{1}$$

where m^p_{mem} and m^p_{aq} are, respectively, the moles of membrane-associated protein and protein in the aqueous buffer, and m_W and m_L are the moles of water and accessible lipid. Eq. 1 is commonly expressed in terms of concentrations:

$$K_x = \frac{[P]_{mem}/[L]_{acc}}{[P]_{aq}/[W]} \tag{2}$$

where $[P]_{\mathrm{aq}}$ and $[P]_{\mathrm{mem}}$ are, respectively, the concentration of free (aqueous phase) and membrane-associated protein,

Please cite this article in press as: Vesga et al., Quantitative characterization of membrane-protein reversible association using FCS, Biophysical Journal (2023), https://doi.org/10.1016/j.bpj.2023.01.026

TABLE 1 Symbols used throughout the text

Symbol	Meaning
A_i	ACF absolute amplitudes
a_i	Probability normalization factor
A, D	Random variables that describe membrane-protein association and dissociation events
B^P_{aq}, B_i	Absolute brightness of fluorescent proteins in solution, brightness of the ith fluorescent species (1 refers to proteins in solution, 2 to protein-carrying vesicles, 3 to free dye)
α, δ	Number of associations and dissociations per vesicle
D	Diffusion coefficient
f^{FCS}_{aq}, f^{FCS}_{mem}	FCS fraction of the protein in solution and partitioned protein, respectively
f_{mem}	Mole fraction of membrane-associated protein
f^{sat}_{mem}	Fraction of membrane-bound protein measured at lipid saturation
$G(\tau)$, $g(\tau)$	Normalized and non-normalized ACF
λ	Average number of membrane-bound proteins per vesicle
K_x	Mole fraction partition coefficient
k_{on}, k_{off}	Association (on) and dissociation (off) rate constants corresponding to individual protein-membrane association/dissociation events
κ	Probability mass function exponential factor
$[L]_{acc}$	Accessible lipid concentration
$[V]$	Concentration of vesicles in solution
$[W]$	Water concentration
m^p_{mem}, m^p_{aq}	Moles of membrane-associated protein, moles of protein in the aqueous buffer
m_W, m_L	Moles of water and accessible lipid
μ	Number of lipids per vesicle
N_{mem}	Discrete random variable for the number of membrane-bound proteins per vesicle
n^P_{Tot}, n^P_{mem}, n^P_{aq}	Total number of proteins, number of proteins associated to the membrane, number of proteins in solution
n^P_i	Number of proteins bound on vesicle i
n^V_{Tot}	Total number of vesicles
n^F, n^F_i	Number of fluorescent particles in the observation volume (index 1 refers to proteins in solution, 2 to protein-carrying vesicles)
$[P]_{Tot}$, $[P]_{aq}$, $[P]_{mem}$	Total concentration of protein at the membrane, concentration of free (aqueous phase), concentration of membrane-associated protein
q_i	Relative brightness of the ith fluorescent species to proteins in solution (1 refers to proteins in solution, 2 to protein-carrying vesicles)
Q	Probability mass function normalization factor
S	Confocal volume dimension ratio ($S = \omega_z/\omega_{xy}$)
τ	ACF lag time
τ_D	Characteristic transit time of the fluorescent particles through the confocal volume
ω_z, ω_{xy}	Axial and lateral dimensions of the confocal volume

$[L]_{acc}$ is the accessible lipid concentration, and $[W]$ is the water concentration ($[W] = 55.5$M at room temperature). Assuming that protein association to the membrane is non-cooperative, the mole fraction of membrane-bound protein, f_{mem}, is

$$f_{mem} = \frac{[P]_{mem}}{[P]_{Tot}} = \frac{K_x[L]_{acc}}{[W] + K_x[L]_{acc}} \quad (3)$$

Using the above definition, K_x is a dimensionless quantity. We note that there are other formalisms in literature for the partition coefficient. These have been discussed thoroughly in (10). Throughout this work we will use K_x and f_{mem} as defined in Eqs. 1–3.

A frequent observation in binding experiments is that protein-membrane binding is not complete even at large lipid concentrations, which results in f_{mem} not reaching 1 asymptotically (e.g., (13,26–28) among many others). This has been ascribed to the presence of a conformer of the protein that is not membrane competent (27) or free fluorescent dye in solution (13), and it has been accounted for introducing an empirical factor, f^{sat}_{mem}, in Eq. 3:

$$f_{mem} = \frac{[P]_{mem}}{[P]_{Tot}} = f^{sat}_{mem}\frac{K_x[L]_{acc}}{[W] + K_x[L]_{acc}} \quad (4)$$

where f^{sat}_{mem} is the fraction of membrane-bound protein measured at lipid saturation (27).

Determination of the protein distribution on lipid vesicles: Statistical equilibrium

Lipids in solution do not organize as a bulk membrane; instead, they self-assemble in the form of lipid vesicles. For this reason, most quantification methods (e.g., (9) and references therein) quantify partitioning by titrating a protein solution with increasing amounts of lipid and estimating the fraction of protein that has partitioned onto the vesicles as a fraction of accessible lipid concentration. Proteins do not distribute homogeneously on the vesicles; rather, every vesicle may carry a different number of protein copies (Fig. 1 *A*) defined by a probability distribution. Thus, in addition to phase equilibrium, statistical equilibrium must also be considered, so that the ratio of protein in solution to membrane-bound protein and the distribution of proteins on vesicles remain constant in time. In phase equilibrium, proteins may dissociate and reassociate from and to the lipid membrane; similarly, in statistical equilibrium, a protein may dissociate from a lipid vesicle and reassociate to a different one, but, importantly, the probability distribution of proteins on vesicles will remain unchanged.

Association of proteins to vesicles is a Poisson process, and it is a common assumption that, upon adding protein to a solution containing lipid vesicles, proteins distribute on the vesicles following a Poisson distribution (13). This assumption holds whenever there are no or few protein dissociation events from the vesicles (11). However, in the general case of reversible protein association (that is, association, dissociation, and reassociation), protein dissociation from the membrane, which is itself a Poisson process too, must also be considered.

Please cite this article in press as: Vesga et al., Quantitative characterization of membrane-protein reversible association using FCS, Biophysical Journal (2023), https://doi.org/10.1016/j.bpj.2023.01.026

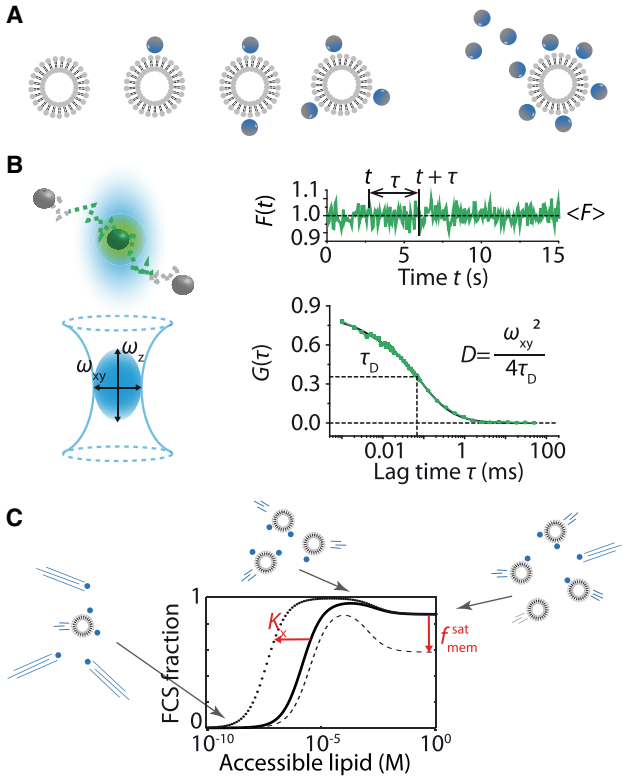

FIGURE 1 Quantification of protein-membrane partitioning using FCS. (*A*) Proteins in solution do not distribute homogeneously on lipod vesicles. Proteins in solution (*blue spheres*) associate with lipid vesicles, which may carry one or several proteins, or none at all. The number of proteins per vesicle in equilibrium is neither homogenous nor random, and is determined by a specific probability distribution. (*B*) FCS explanation. As a fluorescent molecule traverses the confocal volume (*top left*), its fluorescent emission ($F(t)$) is registered in time (*top right*). The time (τ_D) a fluorescent molecule takes to traverse the confocal volume (*bottom left*) is directly related to its diffusion coefficient, D. The ACF ($G(\tau)$)of the emission time-trace (*bottom right*) allows the diffusion coefficient and the average number of molecules in the confocal volume (with dimensions ω_{xy} and ω_z) to be determined. (*C*) FCS titration experiment. The protein-membrane K_x can be determined by titrating the protein with different amounts of lipid that self-assembles in vesicles in an aqueous buffer. The FCS fraction of partitioned protein is measured for every lipid concentration, and K_x and f^{sat}_{mem} are determined from the FCS titration curve using Eq. 29. The different features of the FCS titration curve reflect both the protein partitional behavior and the distribution of the proteins on vesicles. To see this figure in color, go online.

Association and dissociation events are described by random Poisson variables A and D with probability mass function (pmf) $P(A;\alpha)$ and $P(D;\delta)$, where $\alpha(t)$ and $\delta(t)$ are the number of associations and dissociations per vesicle. At any given time, the resulting distribution of proteins on vesicles (N_{mem}) is given by the subtraction of A and D, conditioned to the physical limitation that no dissociation can occur from a vesicle with no proteins attached to it. The expected value of the number of associated proteins per vesicle is $\mathrm{E}[N_{\mathrm{mem}}] = \alpha(t) - \delta(t) = \lambda(t)$. It is worth noting that N_{mem} is not Poisson distributed because the subtraction of Poisson random variables is not another Poisson variable. In addition, association and dissociation are not generally independent, since dissociation may depend on previous association events, resulting in a complex pmf. In the upcoming section, we address the pmf at protein-vesicle equilibrium (section "distribution of proteins on vesicles in statistical equilibrium"). The pmf that describes the time evolution before equilibrium does not generally have a closed solution; as a consequence, we only address a particular case given certain assumptions in section "dynamic distribution of proteins on vesicles."

Distribution of proteins on vesicles in statistical equilibrium

When the protein-vesicle system achieves phase equilibrium, a subset of proteins will remain in solution, whereas the rest will be attached to the lipid vesicles, as determined by K_x. In phase equilibrium, the rates of protein association and dissociation to and from the membrane are equal and therefore the expected number of membrane-associated proteins, $\lambda(t) = \alpha(t) - \delta(t)$, remains constant over time, $\lambda \equiv \lambda(t)$. At any given time, the number of membrane-associated proteins fluctuates around λ, meaning that, as one protein dissociates from a vesicle, another (or the same) protein associates to the same or a different vesicle. Importantly, as the specific vesicle to which the molecule associates is, in general, different, this exchange modifies the distribution of proteins on vesicles until the protein-vesicle system reaches statistical equilibrium. From this point on, the distribution of proteins on vesicles remains constant over time, implying that both the expected value and the variance are also constant over time.

To determine the probability distribution of proteins on vesicles in equilibrium, we consider an isolated system of lipid vesicles in phase and statistical equilibria with freely diffusing proteins in an aqueous solution. Proteins can associate and subsequently dissociate from the vesicles, but, being an isolated system, the amounts of protein and lipid are fixed. Importantly, in this system, the number of lipid vesicles is also fixed (that is, vesicles cannot undergo fusion of fission). Such a system has a fixed partition coefficient K_x.

In this system, all vesicles are identical to each other, and all proteins too. Therefore, for a given number of vesicle-attached proteins, all microscopic arrangements of proteins on vesicles are equally likely. The total number of proteins is conserved, and we assume that this number is sufficiently large so that, when a protein in solution binds to a particular vesicle, it does so at the expense of the remaining protein in solution without depleting it, and does not influence the proteins already associated to the rest of the vesicles. In addition, we assume that proteins already bound to a vesicle do not influence other proteins associating to the same vesicle. Under these two assumptions, lipid vesicles are independent of each other and there is no constraint on several vesicles carrying exactly the same number or protein copies. As a consequence, the probability $P(N_{mem} = n;\kappa)$ of finding a vesicle with n proteins associated to it when the

Please cite this article in press as: Vesga et al., Quantitative characterization of membrane-protein reversible association using FCS, Biophysical Journal (2023), https://doi.org/10.1016/j.bpj.2023.01.026

system is in phase and statistical equilibrium has a decreasing exponential functional form,

$$P(N_{mem} = n;\kappa) = \frac{1}{Q}e^{\frac{-n}{\kappa}} \quad (5)$$

where $Q = \sum_{m=0}^{\infty} e^{\frac{-m}{\kappa}}$ is a normalization factor that stems from the fact that the sum of all probabilities of finding proteins associated to vesicles must add up to 1, and κ is a characteristic parameter of the system, with $\kappa > 0$ to satisfy that the number of vesicles carrying an increasingly large number of proteins tends to 0. A complete derivation of the exponential functional form of $P(N_{mem} = n;\kappa)$ can be found in the Supporting material.

Q is a geometric series with coefficient 1 and ratio $r = \exp(-1/\kappa)$, which is always smaller than 1 since κ is positive. Thus, this series converges to the sum

$$Q = \frac{1}{1 - e^{\frac{-1}{\kappa}}} \quad (6)$$

We rely on physical arguments to find out how parameter κ relates to the system. In equilibrium, the association and dissociation rates are the same and thus, the number of vesicle-bound proteins per vesicle, $\lambda(t)$, fluctuates around its average value λ, which is the expected number of proteins per vesicle:

$$\mathrm{E}[N_{mem}] = \lambda \quad (7)$$

with

$$\lambda = \frac{n^P_{mem}}{n^V_{Tot}} = \frac{[P]_{mem}}{[V]} \quad (8)$$

where $[V]$ is the concentration of vesicles in solution.

By definition, $E[N] = \sum_{m=0}^{\infty} m \cdot P(N = m;\kappa)$. Substituting P and Q from Eqs. 5 and 6 and taking advantage of the convergence properties of the polylogarithm of order -1 ($\mathrm{Li}_{-1}(p) = \sum_k kp^k$, with $\mathrm{p} = \exp(-1/\kappa)$),

$$\mathrm{E}[N_{mem}] = \frac{e^{\frac{-1}{\kappa}}}{1 - e^{\frac{-1}{\kappa}}} = \lambda \quad (9)$$

Solving for κ, $\kappa = 1/[\log(1+\lambda^{-1})]$ and substituting in Eq. 6 yields $Q = \lambda + 1$. Finally, substituting κ and Q in Eq. 5, the probability of finding n proteins on a vesicle is given by

$$P(N_{mem} = n;\lambda) = \frac{\lambda^n}{(\lambda+1)^{n+1}} \quad (10)$$

where λ is the average number of proteins per vesicle, which is itself determined by K_x.

To fully describe the pmf, we still need to calculate its variance. By definition, $\mathrm{var}[N] = \mathrm{E}[N^2] - (\mathrm{E}[N])^2$, with $\mathrm{E}[N^2] = \sum_{m=0}^{\infty} m^2 \cdot P(N = m;\kappa)$. Taking into account in this case the convergence properties of the polylogarithm of order -2 ($\mathrm{Li}_{-2}(p) = \sum_k k^2 p^k$), the variance of the pmf is

$$\mathrm{var}[N_{mem}] = \lambda(\lambda+1) \quad (11)$$

Dynamic distribution of proteins on vesicles

As explained above, association and dissociation are not independent events, since dissociation may depend on previous association events, resulting in a complex pmf. It is possible to find a closed solution for the pmf that describes the time evolution before equilibrium with certain assumptions: 1) the number of protein copies in solution is much larger than the number of vesicles, so a protein is always available in solution for association; and 2) the probability of association is sufficiently larger than the probability of dissociation, implying that dissociation is not limited by association. In this case, association and dissociation can be considered independent Poisson-distributed events and the resulting distribution of protein on vesicles is given by the Skellam distribution (29):

$$P(N_{mem} = n;\alpha,\delta) = e^{-(\alpha+\delta)} \cdot \left(\frac{\alpha}{\delta}\right)^{\frac{n}{2}} \cdot I_{|n|}\left(2\sqrt{\alpha\cdot\delta}\right) \quad (12)$$

where $I_n(z)$ is the modified Bessel function of the first kind. Eq. 12 satisfies that $\mathrm{E}[N_{mem}] = \alpha - \delta$.

Determination of K_x using FCS

Effect of the statistical distribution of protein on vesicles in FCS measurements

The partitional behavior of proteins on the bilayer was studied through the quantification of the fraction of free protein in solution and vesicle-associated protein as they diffuse in solution using FCS (Fig. 1 *B*). FCS is a single-molecule-sensitivity technique that allows the diffusion coefficient of a fluorescent particle to be determined in solution as it traverses a fl-size volume defined by the confocal excitation/detection volume (15,16). When two fluorescent species diffuse together with largely different diffusion coefficients, such as a small protein and a large vesicle carrying protein on its surface, FCS allows the fraction of the fast- and slow-diffusing species to be determined with high accuracy. In the following section, we expand upon the formulation presented in (13,16).

The normalized autocorrelation function, or simply the autocorrelation function (ACF), of a single fluorescent species diffusing in solution is

$$G(\tau) = \frac{1}{n^F}\left(1 + \frac{\tau}{\tau_D}\right)^{-1}\left(1 + \frac{\tau}{S^2\tau_D}\right)^{-\frac{1}{2}} \quad (13)$$

where n^F is the number of fluorescent particles in the observation volume, τ is the ACF lag time, and τ_D is the characteristic transit time of the particles as they traverse the confocal volume with axial and lateral dimensions, ω_z and ω_{xy}. S is the dimension ratio ($S = \omega_z/\omega_{xy}$) and the diffusion coefficient is defined by

Please cite this article in press as: Vesga et al., Quantitative characterization of membrane-protein reversible association using FCS, Biophysical Journal (2023), https://doi.org/10.1016/j.bpj.2023.01.026

$$D = \frac{\omega_{xy}^2}{4\tau_D} \tag{14}$$

Fluorescently tagged protein in solution and protein-loaded vesicles are fluorescent species with different diffusion coefficients due to their different sizes. In general, species will also have different brightness due to every vesicle carrying a different number of fluorescently tagged proteins. In this case, the system ACF is the linear combination of the ACF of the different species, $G_i(\tau)$, weighted by their absolute molecular brightness B_i (16):

$$G(\tau) = \frac{1}{\left[\sum_{\mathrm{i}=1}^{M} B_\mathrm{i} n_i^F\right]^2} \cdot \sum_{i=1}^{M} {B_\mathrm{i}}^2 {n_i^F}^2 G_i(\tau) \tag{15}$$

where n_i^F is the average number of fluorescent particles in the observation volume. The index i identifies the diffusing species, with 1 referring to proteins freely diffusing in solution and 2 to protein-loaded vesicles. When the amount of free dye present in solution is so small that can be neglected, only free protein and protein-loaded vesicles need to be considered, and the upper bound of the summation is $M = 2$; otherwise, free dye in solution will be referred to as index 3 (with $M = 3$).

The molecular brightness is a key parameter in FCS experiments. It defines the number of photons emitted by molecules of different species as they traverse the observation volume (Fig. 1 *B*). Equation 15 highlights the critical role this parameter plays as the contribution of each species to the ACF is not linear with brightness, but depends, instead, on the square of the brightness parameter. This implies that, relative to a vesicle carrying a single copy of the protein, a vesicle carrying two protein copies will have a fourfold contribution to the measured ACF, a vesicle carrying three protein copies will have a ninefold contribution, and so on. In this system, protein-loaded vesicles each have different brightness according to the distribution of protein on vesicles and will, therefore, contribute differently to the ACF.

It is highly advantageous to formulate Eq. 15 in terms of the relative molecular brightness, q:

$$q_i = \frac{B_i}{B_{aq}^P} \tag{16}$$

where the index refers to the species and B_{aq}^P is the absolute molecular brightness of free proteins in solution. Thus, $B_1 \equiv B_{aq}^P$. As a consequence, $q_1 = 1$ and q_2 is proportional to the number of fluorescent protein copies carried by the vesicle. Since vesicle brightness is proportional to the number of proteins associated to it, the relative molecular brightness follows the probability distribution of proteins on vesicles (Eq. 10). Eq. 15 can now be formulated in terms of q:

$$G(\tau) = \frac{1}{\sum_i \langle q_i \rangle n_i^F} \sum_i A_i g_i(\tau) \tag{17}$$

where <> denotes average value, and A_i are the absolute amplitudes of each species contributing to the ACF:

$$A_i = \frac{\langle {q_i}^2 \rangle \, n_i^F}{\sum_i \langle q_i \rangle n_i^F} \tag{18}$$

and $g_\mathrm{i}(\tau)$ is the non-normalized ACF corresponding to each species:

$$g_i(\tau) = \left(1 + \frac{\tau}{\tau_{D_i}}\right)^{-1} \left(1 + \frac{\tau}{S^2 \tau_{D_i}}\right)^{-\frac{1}{2}} \tag{19}$$

Determination of the partitioned protein fraction

It is often convenient to formulate Eq. 17 in terms of fractional amplitudes, f_i, contributing to the ACF:

$$G(\tau) = \frac{1}{\langle n^F \rangle} \sum_i f_i \cdot g_i(\tau) \tag{20}$$

where $\langle n^F \rangle$ is the brightness-weighted average number of fluorescent particles (proteins in solution and protein-carrying vesicles) in the observation volume: $\langle n^F \rangle = \left(\sum_\mathrm{i} \langle q_i \rangle n_i^F\right)^2 / \sum_\mathrm{i} \langle {q_i}^2 \rangle n_i^F$, and f_i is the contribution of each fluorescent species to the ACF:

$$f_i = \frac{A_i}{\sum_i A_i} = \frac{\langle {q_i}^2 \rangle n_i^F}{\sum_i \langle {q_i}^2 \rangle n_i^F} \tag{21}$$

with $\sum_i f_i = 1$. For the sake of clarity, we will refer to the fractional ACF amplitudes f_i as FCS fractions.

As stated above, index 1 refers to the free protein in solution and index 2 to protein-loaded vesicles. Thus, $q_1 = 1$. Without loss of generality, we will assume that protein association to the membrane does not modify the probe's quantum yield, and thus q_2 is directly the number of protein copies on protein-carrying vesicles, which is governed by the probability distribution of protein on vesicles. Equation 21 does not presume any particular distribution of proteins on vesicles. In the case of reversible association, the pmf of protein on vesicles is given by Eq. 10. Importantly, however, although Eq. 10 is defined for all the vesicles in solution irrespective of whether or not they carry protein, vesicles that do not carry proteins are not fluorescent, and thus are not accounted for in the ACF calculation (Eq. 20). We can therefore compute the average quantities $\langle q_2 \rangle$ and $\langle {q_2}^2 \rangle$ in Eq. 21 as the overall quantity divided by the number of protein-carrying vesicles. Recalling Eqs. 9 and 11,

Please cite this article in press as: Vesga et al., Quantitative characterization of membrane-protein reversible association using FCS, Biophysical Journal (2023), https://doi.org/10.1016/j.bpj.2023.01.026

$$\langle q_2 \rangle = \frac{\mathrm{E}[N] n_{Tot}^V}{n_2^F} = \frac{\lambda n_{Tot}^V}{n_2^F} \tag{22}$$

$$\langle {q_2}^2 \rangle = \frac{\mathrm{E}\left[N^2\right] n_{Tot}^V}{n_2^F} = \frac{\left(\lambda(\lambda+1)+\lambda^2\right) n_{Tot}^V}{n_2^F} \tag{23}$$

where n_{Tot}^V is the total number of vesicles.

The FCS fractions f_1 and f_2 in Eq. 21 can now be calculated and endowed with a clearer physical meaning. Interpretation of the FCS fraction f_1 is straightforward as f_1 is the contribution of protein in the aqueous buffer to the ACF. Following the notation above, $f_{aq}^{FCS} \equiv f_1$. To understand the physical meaning of f_2, we again take into account that vesicles that do not carry proteins do not contribute to the ACF. As a consequence, the contribution of protein-carrying vesicles to the ACF is strictly determined by the proteins bound to the membrane. This implies that f_2 fully carries the information for the membrane-bound protein and can be interpreted as the partitioned protein FCS fraction. Following the notation above, f_2 can now be termed as f_{mem}^{FCS}. Using Eqs. 22 and 23,

$$f_{aq}^{FCS} = \frac{n_{aq}^P}{n_{aq}^P + \lambda(2\lambda+1)\cdot n_{Tot}^V} \tag{24}$$

and

$$f_{mem}^{FCS} = \frac{\lambda(2\lambda+1)\cdot \mathrm{n}_{Tot}^V}{\mathrm{n}_{aq}^P + \lambda(2\lambda+1)\cdot n_{Tot}^V} \tag{25}$$

where we have assumed that the number of non-fluorescent protein copies is negligible and thus n_1^F is equal to the number of proteins in aqueous solution n_{aq}^P.

If the probe quantum yield changes upon membrane binding, q_2 would be linearly proportional to the number of proteins on the vesicle and a proportionality constant would have to be introduced in Eqs. 22 and 23.

FCS fractions f_{aq}^{FCS} and f_{mem}^{FCS} represent the contribution of the freely diffusing protein and membrane-bound protein to the ACF curve, which is the mole fraction weighted by the species brightness considering the distribution of proteins on vesicles. The mole fraction of bound protein, f_{mem}, can be determined from either f_{aq}^{FCS} or f_{mem}^{FCS}, recalling that the average value of membrane-associated protein, λ, is just the ratio of membrane-bound protein to total vesicle concentration (Eq. 8), and thus

$$f_{mem} = \lambda \frac{[V]}{[P]_{total}} \tag{26}$$

with

$$[V] = \frac{2\cdot[L]_{\mathrm{acc}}}{\mu} \tag{27}$$

where $[V]$ is the concentration of vesicles in solution, $[L]_{\mathrm{acc}}$ is the concentration of protein-accessible lipid, and μ is the number of lipids per vesicle.

Determination of the molar partition coefficient $\mathrm{K_x}$

The molar partition coefficient K_{x} is determined from the FCS fractions f_{aq}^{FCS} and f_{mem}^{FCS} obtained titrating the protein in solution with an increasing concentration of lipid. The observed f_{aq}^{FCS} and f_{mem}^{FCS} can be expressed in terms of the experimentally accessible concentrations of protein and lipid dividing numerator and denominator by the total volume and substituting λ as a function of K_{x} and f_{mem}^{sat} using Eqs. 4, 26, and 27:

$$f_{aq}^{FCS} = \frac{\left(1 - f_{mem}^{sat}\right)K_x^2[L]_{acc}^2 + \left(2 - f_{mem}^{sat}\right)[W]K_x[L]_{acc} + [W]^2}{{K_x}^2{[L]_{acc}}^2 + \left(2[W]K_x + {f_{mem}^{sat}}^2{K_x}^2[P]_{\mathrm{Tot}}\mu\right)[L]_{acc} + [W]^2} \tag{28}$$

and

$$f_{mem}^{FCS} = \frac{f_{\mathrm{mem}}^{\mathrm{sat}}K_{\mathrm{x}}^2[L]_{\mathrm{acc}}^2 + \left(\mathrm{f}_{\mathrm{mem}}^{sat}[W]\mathrm{K_x} + {f_{\mathrm{mem}}^{\mathrm{sat}}}^2{K_{\mathrm{x}}}^2[P]_{\mathrm{Tot}}\mu\right)[L]_{\mathrm{acc}}}{{K_{\mathrm{x}}}^2{[L]_{\mathrm{acc}}}^2 + \left(2[W]K_x + {f_{\mathrm{mem}}^{\mathrm{sat}}}^2{K_{\mathrm{x}}}^2[P]_{\mathrm{Tot}}\mu\right)[L]_{\mathrm{acc}} + [W]^2} \tag{29}$$

Finally, K_{x} (and f_{mem}^{sat}) can now be determined fitting Eqs. 28 or 29 to f_{aq}^{FCS} or f_{mem}^{FCS} empirically obtained from the FCS titration curve.

MATERIALS AND METHODS

Modeling protein-membrane association/dissociation dynamics

We modeled protein-membrane partitioning as a reaction-diffusion process described by the reaction-diffusion master equation (RDME), which determines the probability of a reaction or a diffusion event. We used a representation that does not make any assumption on the binding stoichiometry and that does not limit the number of proteins associating to the vesicle. As a consequence, the number of free sites does not decrease upon protein binding.

We simulated stochastic reaction-diffusion trajectories, which is equivalent to numerically solving the RDME (30,31). We used a group of computational methods to simulate the trajectories of the stochastic protein membranes system: linked-list cells for the spatial description of particles in boxes (32,33), periodic boundary conditions for positions, next reaction method for simulating the reactions (31), and next subvolume method (34–37) for simulating diffusion events. The detailed description of the method and the pseudo-code algorithm can be found in the section "extended methods" in the Supporting material accompanying this paper.

Please cite this article in press as: Vesga et al., Quantitative characterization of membrane-protein reversible association using FCS, Biophysical Journal (2023), https://doi.org/10.1016/j.bpj.2023.01.026

Computational microscopy

Brownian dynamics simulations

We used Brownian molecular dynamics to simulate the diffusion of proteins and vesicles with enough spatial and temporal resolution to perform a computational microscopy experiment (38). Proteins and vesicles were simulated in Gromacs as spherical particles. To calibrate the friction coefficient for each type of particle, we initially set the Gromacs-parametrized friction coefficient to 0, and then modified independently the thermostat time constant for each type of particle to obtain a friction coefficient so that the particles Brownian diffusion coefficient $D = \langle r^2 \rangle / 4t$ matched the empirical one obtained by FCS experiments. A detailed description of the method can be found in the section "extended methods" in the Supporting material.

Computational FCS

To perform a computational FCS experiment, we simulated the excitation/detection process of diffusing fluorescent particles as they traverse a confocal volume. To this end we used the finely sampled trajectories obtained using Gromacs and simulated the emission/detection process. The excitation/detection process was simulated assuming a spatially Gaussian-distributed excitation probability that matches the empirical point spread function (PSF) for every molecule located within the excitation/detection volume (see section "materials and methods"). Poisson statistics were assumed for the detection process. The detailed description of the method and a pseudo-code algorithm can be found in the section "extended methods" in the Supporting material. We finally performed the same FCS analysis on the simulated data as on the empirical data (see below).

Estimation of the CRB for K_x determination using FCS

The minimal variance of an unbiased estimator $\widehat{\theta}$ for a parameter θ is determined by the reciprocal Fisher information matrix (FIM), $\mathscr{I}(\theta)$, $\mathrm{var}[\widehat{\theta}] \geq \mathscr{I}(\theta)^{-1}$, where the function $1/\mathscr{I}(\theta)$ the CRB on the variance of the unbiased estimator of θ. For this study, the parameters that we have estimated are K_x and f_{mem}^{sat}, the independent variables are $[P]_{\mathrm{Tot}}$ and $[L]_{\mathrm{acc}}$, and the experimental observations are either f_{aq}^{FCS} or f_{mem}^{FCS}, modeled by Eq. 24 and Eq. 25, respectively. We have derived the functional form of the CRB on the variance of K_x and f_{mem}^{sat}, where the FIM is obtained taking the partial derivatives of f_{aq}^{FCS} or f_{mem}^{FCS} with respect to K_x and f_{mem}^{sat}. A detailed description of the derivation of the FIM and the exact functional form for the CRB on the variance of K_x and f_{mem}^{sat} is given in the Supporting material.

Materials

1-Palmitoyl-2-oleoyl-glycero-3-phosphocholine (POPC), 1-palmitoyl-2-oleoyl-sn-glycero-3-phospho-L-serine (POPS), and cholesterol (Chol) were purchased from Avanti Polar Lipids (Birmingham, AL, USA). Phospholipid stock concentrations were determined by the Fiske and Subbarow phosphate assay method. 10E8-3R Fabs were labeled with Abberior KK114 (Abberior, Göttingen).

Sample preparation

Antibody purification and labeling

The purified KK114-labeled 10E8-3R Fab was kindly provided by Prof. Jose Luis Nieva (University of the Basque Country, Spain). Purification and labeling procedures have been previously described elsewhere (22).

Preparation of model membranes (LUVs)

Large unilamellar vesicles (LUVs) made of a lipid mixture of POPC, Chol, and POPS were produced following the extrusion method. The lipid mixtures were mixed from chloroform lipid stocks and dried under vacuum conditions. They were re-suspended in HEPES buffer at 50°C and vortexed, forming multi-lamellar vesicles (MLVs). Subsequently, 10 freeze-thaw cycles were performed to the suspension of MLVs. The solution was extruded 10 times through two stacked polycarbonate membranes with a nominal pore-size of 0.1 μm to obtain 100-nm LUVs. It was estimated that there were approximately 10^5 lipid molecules per vesicle, calculated assuming the average area per lipid is 65 Å^2 (39) and that both leaflets of the vesicle bilayer accommodate the same number of lipid molecules.

FCS

Optical setup

A detailed description of the optical set up can be found in (40). In brief, excitation and detection were performed through a water immersion objective HCX PL APO 63×/1.20 W CORR Lbd Bl (Leica) on a confocal Leica SP5. KK114-labeled samples were excited at 633 nm, and their fluorescent emission was registered on the Avalanche Photodiodes (APD) through a BP647-703 filter. The average power density at the sample plane was 50 kW/cm^2. Photon arrival times were recorded using a SPC830 TCSPC card (Becker & Hickl, Berlin), which also registered the pixel, line, and frame signals from the microscope scanner. The whole system was externally clocked at 20 MHz. The SPC830 binary output files were decoded using an in-house developed Matlab routine.

FCS titration experiment

A 25 nM solution of fluorescently labeled Fab was titrated with increasing lipid concentration (from 10^{-12} M to 2×10^{-7} M). For every lipid concentration, an FCS autocorrelation trace was calculated. The effect of bright aggregates was minimized by applying an intensity threshold on the time-photon trace and a variance filter on the autocorrelation trace (see Supporting material). f_{mem}^{FCS} was determined as explained below. For every lipid concentration, three FCS measurements (45 s each) were carried out. Measurements were repeated three times with independent samples.

Determination of the partition coefficient by FCS

The experimental procedure to determine K_x and f_{mem}^{sat} can be summarised in five steps: 1) Determine the diffusion coefficient of free protein in solution (D_1) using a sample with no lipid; determine the diffusion coefficient of vesicles in solution (D_2) using a sample with no protein. Vesicles can be labeled with a hydrophobic probe (in this work we used DOPE-KK114) incorporated during LUV reconstitution, so that it distributes homogeneously through the vesicles. 2) Vesicle fusion or fission should be ruled out at this point: perform FCS to determine vesicle concentration and vesicle diffusion coefficient at different points in time. In the absence of vesicle fusion or fission, both parameters remain constant over time. Proteins may promote vesicle fusion, so this test should be performed in the presence of proteins. 3) Titrate the protein solution with different lipid (LUV) concentrations and perform FCS at each one. 4) Fit Eq. 20 to the experimental ACF obtained for different LUV concentrations to compute f_{mem}^{FCS}. Use D_1 and D_2 obtained above to reduce the number of fitting parameters. 5) Fit Eq. 29 to the obtained f_{mem}^{FCS} as a function of accessible lipid concentration with fitting parameters K_x (and f_{mem}^{sat} if required). 6) Compute the uncertainty for the fitting parameters K_x and f_{mem}^{sat} either by support plane analysis (SPA) (41) or repetition of experiments. Fitting software was developed in the laboratory in Matlab and is available at https://github.com/cnbbiophot/fitting-gui

Please cite this article in press as: Vesga et al., Quantitative characterization of membrane-protein reversible association using FCS, Biophysical Journal (2023), https://doi.org/10.1016/j.bpj.2023.01.026

RESULTS

Probability distribution of proteins on vesicles

Having derived the theoretical pmf for proteins that reversibly associate to lipid vesicles, we first validated it through an in silico experiment. To this end, we modeled the dynamics of proteins and vesicles in solution using a reaction-diffusion (RD) stochastic simulation. Our RD modeling does not presume any particular probability distribution of proteins on vesicles (see section "materials and methods"). Instead, it simulates Brownian diffusion and association and dissociation events given the diffusion coefficient of both vesicles and proteins and the microscopic association and dissociation rate constants. The diffusion coefficients of the vesicles and proteins were previously experimentally characterized by FCS on independent solutions ($D_1 = 90$ μm^2 s^{-1}, $D_{Ves} = 5$ μm^2 s^{-1}). Given that the diameter of the lipid vesicles ($\approx$100 nm) is more than one order of magnitude larger than that of proteins, we assumed that protein-loaded vesicles diffused with the same diffusion coefficient as naked vesicles (and thus $D_{Ves} = D_2$). The association rate constant ($k_{on} = 10^9$ $M^{-1}s^{-1}$) was chosen so that the reaction rate was diffusion limited and the dissociation rate k_{off} was chosen to reproduce different physiological K_x.

We first showed that the protein-vesicle mixture reached both phase and statistical equilibria. Fig. 2 shows the dynamics of proteins and vesicles as they diffuse in a 3D volume, associate, and dissociate, eventually reaching phase and statistical equilibria. Initially ($t = 0$ s), proteins and vesicles are randomly distributed; they are not associated, and they diffuse freely within the simulation 3D volume. Upon a protein-vesicle encounter, successful association can occur, determined by k_{on}. Given that, initially, all proteins are free, associations must start building up before any dissociation can occur (Fig. 2 *A*, dotted blue line). In turn, dissociations will occur at a rate determined by k_{off} (Fig. 2 *A*, solid red line). Phase equilibrium is achieved when the rate of association and dissociation are equal (the solid and dotted lines in Fig. 2 *A* have equal slope) and the fraction of free protein remains stationary from approximately 10 s onward after the onset of protein and vesicle diffusion (inset). At this point, the population of vesicle-associated protein does not increase any further and fluctuates around its average value determined by K_x.

Statistical equilibrium is achieved when the mean and the variance of the distribution of proteins on vesicles are stationary. This is illustrated in Fig. 2 *B* and *C*. The average number of vesicle-bound proteins per vesicle (λ) reaches a stationary value (dashed green line) at about 10 s into the simulation (Fig. 2 *B*), consistent with the phase equilibrium dynamics. Interestingly, even when phase equilibrium has been reached, membrane-bound proteins keep dissociating and re-associating to the same or a different vesicle, so that the distribution of protein on vesicles evolves in time

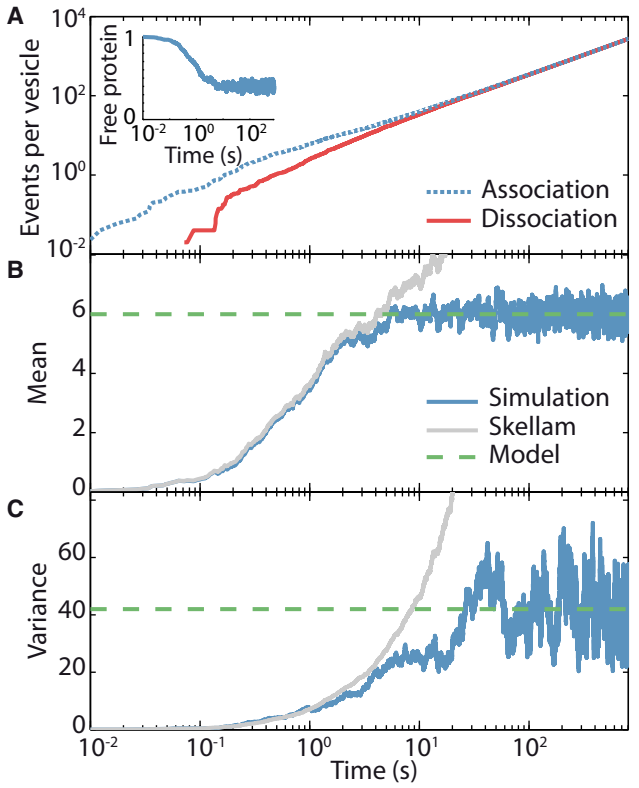

FIGURE 2 Proteins and vesicles dynamics as they associate, dissociate, and reassociate. (*A*) Association $\alpha(t)$ and dissociation $\delta(t)$ events per vesicle as a function of time. Phase equilibrium is reached when both curves have equal slope. (*B*) Mean number of membrane-bound proteins per vesicle, $\lambda(t) = \alpha(t)$-$\delta(t)$. The solid blue line is $\lambda(t)$, obtained from the simulation ensemble (sample mean). The dashed green line is the expected membrane-bound particles per vesicle in equilibrium $E[N_{mem}]$ as calculated from the pmf derived in this work (Eq. 9). In equilibrium, $\lambda(t)$ computed from the simulation matches $E[N_{mem}]$. The out-of-equilibrium $\lambda(t)$ (*light line*) can be approximated by the Skellam distribution (Eq. 12). (*C*) Variance of the distribution of membrane-bound proteins on vesicles. The solid blue line is the sample variance computed from the simulated data; the dashed green line is the variance derived from the pmf (Eq. 11). Statistical equilibrium is defined by stationary sample average and variance. The pmf variance and the sample variance match in statistical equilibrium. The out-of-equilibrium variance can be approximated by the Skellam distribution (*light line*). To see this figure in color, go online.

until the system reaches statistical equilibrium. This means that the shape of the distribution continues evolving, as proved by the increasing variance (Fig. 2 *C*), until the variance reaches the value given by Eq. 11 (dashed green line). Fig. 2 shows that the dynamics of protein binding to the membrane and the distribution of proteins on vesicles are different, since any given number of proteins can be distributed differently on the vesicles. Although the time it takes to reach phase equilibrium essentially depends on the concentration of protein and vesicles and their diffusion coefficients, the time it takes to reach statistical equilibrium is highly dependent on the initial localization of proteins and vesicles within the solution volume. Fig. 2 *B* and *C* also shows that the out-of-equilibrium distribution of

Please cite this article in press as: Vesga et al., Quantitative characterization of membrane-protein reversible association using FCS, Biophysical Journal (2023), https://doi.org/10.1016/j.bpj.2023.01.026

vesicle-bound proteins can be approximated by Eq. 12 (gray line).

Having shown that the RD simulation reproduced the dynamic behavior of proteins associating and dissociating from lipid vesicles predicted in the theory section (Eqs. 10 and 12), we studied the effect of reversible association on the distribution of protein on lipid vesicles in equilibrium. To this end, we compared the distribution of proteins on vesicles for three cases that mimic physiological protein-membrane dissociation using their characteristic k_{off}. First we studied the case of a reversible interaction subject to strong dissociation ($k_{off} \approx 5\ s^{-1}$), such as that of an HIV antibody with a viral membrane, which is mainly driven by electrostatic attraction and weak hydrophobic anchoring (4); then, we studied an interaction subject to weak dissociation ($k_{off} \approx 5 \times 10^{-3}\ s^{-1}$), such as the highly specific association of an HIV antibody with its epitope, with k_{off} in the order of 10^{-5} to $10^{-2}\ s^{-1}$(42–44). Finally, we studied the case of non-reversible association ($k_{off} \approx 0\ s^{-1}$). Fig. 3 *A* shows the dynamics of the fraction of partitioned protein in the protein-vesicle mixture as it reaches equilibrium. In equilibrium, a larger k_{off} results in a smaller fraction of protein associated to the membrane (solid blue line, $k_{off} \approx 5\ s^{-1}$), whereas, as expected, all the protein is associated to the membrane when the association is not reversible (dotted green line, $k_{off} \approx 0\ s^{-1}$). For weak dissociation (dashed red line, $k_{off} \approx 5 \times 10^{-3}\ s^{-1}$), the association dynamics are reasonably similar to the case of irreversible partitioning and virtually all the protein is associated to the membrane when the system is given enough time. For all cases, the average number of protein copies per vesicle is $\lambda = 2$. Significantly, not only does k_{off} determine the presence of free protein in the aqueous phase in equilibrium but it also determines the distribution of protein on the vesicles constituting the lipid phase. Fig. 3 *B–D* show the distribution of the protein on the vesicles. Fig. 3 *B* and *C* demonstrate that, when the protein is allowed to dissociate and reassociate (non-zero k_{off}), it distributes on the vesicles following the probability distribution derived in the section "theory" (Eq. 10). It is only when the association is not reversible (Fig. 3 *D*) that the behavior is Poissonian. Fig. 3 *C* and *D* demonstrate that, although the average number of proteins per vesicle is virtually the same for weak dissociation (Fig. 3 *C*) and no dissociation (Fig. 3 *D*), the distribution of proteins on vesicles is radically different.

Determination of K_x of reversible protein-membrane association using FCS titration experiments

Once we had established the probability distribution for the reversible association of proteins on lipid vesicles, we accurately quantified the K_x of the association using FCS. Using FCS, the partition coefficient, K_x, and the fraction of membrane-bound protein at lipid saturation, f_{mem}^{sat}, can be determined from a titration experiment (Fig. 1 *B* and *C*). FCS has previously been used to quantify K_x with high accuracy in the case of non-reversible association (11,13,17,18,20). Still, to our best knowledge, reversibility of the association has never been considered for K_x determination using FCS.

To test the suitability of FCS titration experiments for K_x determination of reversible protein-membrane association using the pmf of proteins on vesicles derived in the previous section (Eq. 10), we performed computational FCS experiments, which involved 1) the simulation of the diffusion

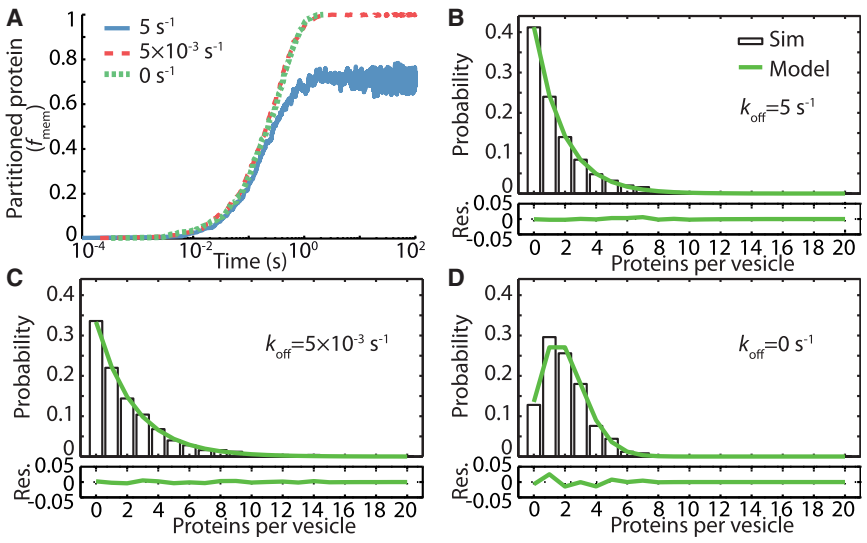

FIGURE 3 Effect of protein-vesicle dissociation and reassociation on the distribution of protein on vesicles. (*A*) Mole fraction of membrane-associated protein in equilibrium (f_{mem}) for different k_{off} ($5\ s^{-1}$, $5 \times 10^{-3}\ s^{-1}$ and $0\ s^{-1}$). A larger k_{off} implies a higher dissociation probability. In equilibrium, all proteins are associated to the vesicles for k_{off} $5 \times 10^{-3}\ s^{-1}$ and $0\ s^{-1}$ ($f_{mem} = 1$), whereas, for $k_{off} = 5\ s^{-1}$, the equilibrium f_{mem} is 0.73. (*B–D*) Distribution of protein on vesicles in statistical equilibrium for (*B*) strong dissociation $k_{off} = 5\ s^{-1}$; (*C*) weak dissociation $k_{off} = 5 \times 10^{-3}\ s^{-1}$, and (*D*) no dissociation $k_{off} = 0\ s^{-1}$. The bars show the frequency of vesicles carrying a certain number of proteins obtained from the simulation data at statistical equilibrium. The lines show the pmf derived in Eq. 10 (*B* and *C*) and a Poisson pmf (*D*). The difference between the theory pmf (Eq. 10 or Poisson) and the simulated distribution is shown below. Note the striking different protein distribution in (*C*) and (*D*) even though the mean number of proteins per vesicle in equilibrium equals two in both cases. In all cases, $k_{on} = 10^{-9}\ M^{-1}\ s^{-1}$; protein concentration, 6.64 nM; lipid concentration, 0.17 mM. To see this figure in color, go online.

Please cite this article in press as: Vesga et al., Quantitative characterization of membrane-protein reversible association using FCS, Biophysical Journal (2023), https://doi.org/10.1016/j.bpj.2023.01.026

of proteins, vesicles, and protein-loaded vesicles distributed in phase and statistical equilibria according to Eq. 10, and 2) the simulation of photon statistics followed by FCS computation with detection parameters analogous to a bench experiment. Simulations were performed at different lipid concentrations, and an f_{mem}^{FCS} value was determined for every lipid concentration fitting Eq. 20 to the ACF. This allowed the calculation of a titration curve, which was correspondingly used to retrieve K_x fitting Eq. 29 to it (Fig. 4 *A*). Computational FCS experiments require fine temporal and spatial resolution. Given the diameter of the vesicles (100 nm), the limited spatial resolution precluded the use of lattice-based methods such as the next subvolume method that we had previously used to study the association/dissociation dynamics. For this reason, particle trajectories were computed using Brownian molecular dynamics, integrating the Langevin equation with a 10-ns time step and saving trajectories every 1 μs. This ensured adequate temporal and spatial sampling. (see sections "materials and methods" and "extended methods" in the Supporting material).

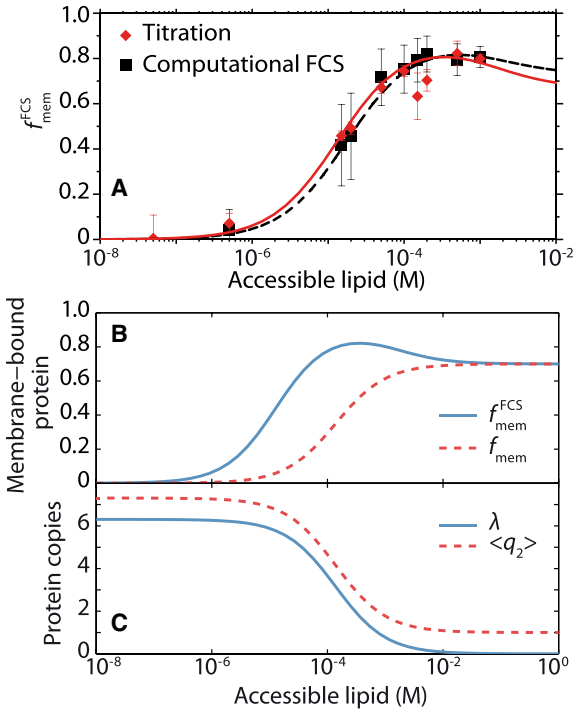

FIGURE 4 FCS titration experiment. (*A*) Empirical (*diamonds*, *solid red line*) and computational FCS (*squares*, *dashed black line*) titration experiments of a 48-kDa protein (10E8-3Rb Fab) that diffuses at 90 $\mu m^2 s^{-1}$ with different amounts of lipid that assemble in 100-nm LUV diffusing at 5 $\mu m^2 s^{-1}$. The experimental data were used as ground truth for the computational FCS titration experiment. The simulation fully matched the experimental data, demonstrating the suitability of FCS titration experiments to quantify K_x. (*B*) The membrane-bound protein FCS fraction, f_{mem}^{FCS}, carries more information than the mole fraction, f_{mem}. In addition to the fraction of partitioned protein, f_{mem}^{FCS} also contains information on the distribution of protein on vesicles. Both quantities converge when lipid vesicles carry, on average, only one protein. (*C*) Mean number of proteins per vesicle, λ, and mean number of proteins per protein-carrying vesicle, $<q_2>$. As the accessible lipid concentration increases and, as a consequence, so does the number of vesicles, both λ and $<q_2>$ decrease. However, although λ converges to 0 for a large number of vesicles, $<q_2>$ converges to 1. To see this figure in color, go online.

The computational FCS experiment confirmed the suitability of FCS titration experiments to quantify protein-membrane K_x in the case of reversible association using the pmf derived in Eq. 10. Fig. 4 *A* shows (diamonds, solid red line) the f_{mem}^{FCS} values for an actual titration experiment of a 48-kDa protein (the 10E8 Fab) with different concentrations of lipid assembled in 100-nm LUV. Eq. 29 was fit to the experimental data, yielding $K_x = 4.0 \times 10^5 \pm 0.6 \times 10^5$ and $f_{mem}^{sat} = 0.69 \pm 0.09$. Fig. 4 also shows (squares, dashed black line) the corresponding data retrieved from a computational FCS experiment using the empirically obtained quantities as the ground truth. Every point in the curve is the average of 30 5-s computational FCS experiments, which were also used to calculate the uncertainty of the simulated data FCS fractions. Fig. 4 *A* shows that the simulation matches the actual experiment, yielding the same values for K_x and f_{mem}^{sat} within the uncertainty ($K_x = 3.6 \times 10^5 \pm 0.8 \times 10^5$ and $f_{mem}^{sat} = 0.69 \pm 0.07$) as those obtained in the actual experiment. The uncertainty for K_x and f_{mem}^{sat} for both actual and simulated data was calculated using support plane analysis (SPA) (41).

Fig. 4 also illustrates the role protein distribution plays in FCS. As the accessible lipid concentration increased, so did f_{mem}^{FCS} until, instead of saturating, it reached a maximum at around 1.2×10^{-4} M before decreasing to f_{mem}^{sat} (Fig. 4 *B*). The presence of a maximum is just the reflection of a non-homogeneous distribution of proteins on vesicles. This maximum is explained considering that f_{mem}^{FCS} is the contribution of vesicle-bound protein to the ACF, and the shape of the curve just reflects the number of vesicles carrying one or more proteins in relation to the number of proteins in solution. Fig. 4 *B* shows the relation of f_{mem}^{FCS} with f_{mem}. Both the FCS fraction (f_{mem}^{FCS}) and the mole fraction (f_{mem}) of membrane-bound protein carry the information on the fraction of partitioned protein. In addition, f_{mem}^{FCS} also contains information on the distribution of protein on vesicles. For this reason, they only overlap at high lipid concentrations, when occupied vesicles carry only one protein, $<q_2> = 1$ (dashed red line, Fig. 4 *C*).

Fig. 4 *C* shows that the average number of proteins per vesicle (λ, solid blue line) used to determine K_x by FCS titration is very low. For this particular experiment, the highest λ corresponded to the minimum lipid concentration used (10^{-8} M), and it was just 6.3 protein copies per lipid vesicle, whereas, at the maximum experimentally accessible lipid concentration (10^{-3} M, Fig. 4 *A*), the vesicles only carried 0.7 protein copies on average. A consequence of the low number of protein copies per vesicle is that protein cooperativity or steric effects at the surface of the vesicles are expected to be minimal.

Please cite this article in press as: Vesga et al., Quantitative characterization of membrane-protein reversible association using FCS, Biophysical Journal (2023), https://doi.org/10.1016/j.bpj.2023.01.026

Optimal determination of the partition coefficient for reversible association using FCS

Once we had validated the use of FCS titration experiments and the pmf of proteins on vesicles (Eq. 10) for K_x determination, we set out to evaluate the accuracy of FCS for the determination of the parameters that describe the association. With this aim, we estimated the CRB on the variance of K_x and f_{mem}^{sat}. The CRB establishes the minimal possible variance of an empirically determined quantity, allowing the experimental interval for optimal K_x estimation to be determined. Thus, we calculated the CRB on K_x and f_{mem}^{sat} within an empirically relevant interval of accessible lipid concentrations (from 10^{-1} to 10^{3} μM) taking into account that FCS observations are normally distributed (see section "materials and methods").

Fig. 5 *A* shows that the K_x interval where the uncertainty for K_x determination is minimal spans three orders of magnitude (K_x between 10^4 and 10^6) irrespective of f_{mem}^{sat}. For K_x smaller than 2×10^3 and larger than 2×10^6, the uncertainty of the determined K_x increases asymptotically. Lower or larger K_x values can, in principle, be determined with non-infinite uncertainty titrating the protein to a different lipid concentration interval. However, this approach is limited by experimental constraints, such as the solubility and concentration of vesicles at high lipid concentration or the appearance of electrostatic screening due to the large number of proteins that populate vesicles at low lipid concentrations. Fig. 5 *B* shows that the CRB on f_{mem}^{sat} variance is roughly flat for all possible f_{mem}^{sat} values ([0,1] interval), although its absolute value is dependent on K_x. This implies that the overall uncertainty in K_x determination using FCS majorly depends on the value of K_x itself, and not f_{mem}^{sat}. We note that the absolute value of the CRB on the variance of K_x and f_{mem}^{sat} depends on the uncertainty in the determination of the FCS fraction of free or partitioned protein (f_{aq}^{FCS} or f_{mem}^{FCS}) at every lipid concentration used for titration. Since FCS measurements are independent, this quantity is normally distributed, and its variance can be decreased by repetition or by increasing the number of points used to determine K_x. A larger or smaller uncertainty in the determination of the fraction of partitioned protein may modify the absolute CRB estimation, but it does not alter the shape of the curve. As a consequence, the optimal interval for K_x and f_{mem}^{max} determination is the same irrespective of the value of the uncertainty of the observed FCS fraction. For this reason, Fig. 5 *A* and *B* have been calculated using empirical representative estimates on f_{mem}^{FCS} variance.

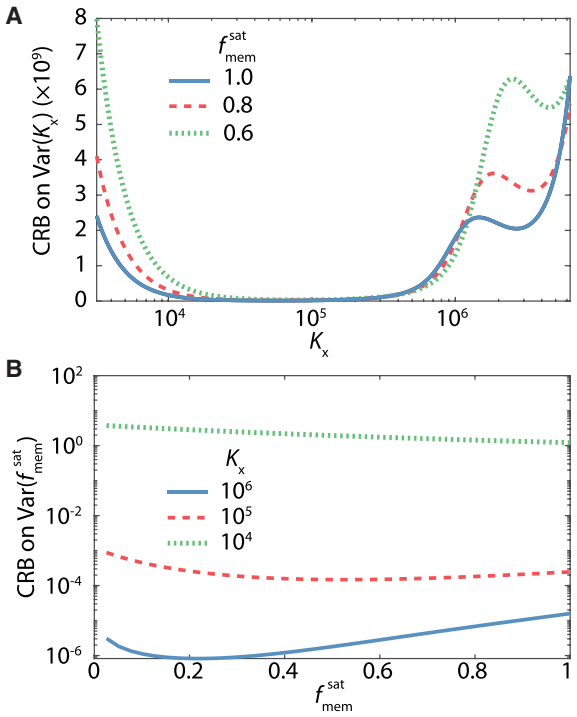

FIGURE 5 Accuracy and limits to K_x determination by FCS titration. (*A*) CRB on K_x variance determined from FCS titration experiments and calculated for different f_{mem}^{sat}. (*B*) CRB on f_{mem}^{sat} variance for different K_x. (*A*) and (*B*)computed using 11 log-spaced points. To see this figure in color, go online.

K_x and f_{mem}^{sat} can be determined from FCS titration experiments using as a readout either f_{aq}^{FCS} or f_{mem}^{FCS}. The use of f_{mem}^{FCS} as a function of accessible lipid produces an increasing curve given by Eq. 29, such as those shown in Fig. 4, whereas f_{aq}^{FCS} results in a decreasing curve (Eq. 28) with less intuitive interpretation. Notwithstanding, the CRB analysis shows that K_x determination using Eq. 28 or Eq. 29 is equivalent in terms of uncertainty (Fig. S1).

10E8-3R association to the membrane

Having determined the optimal region for the quantification of reversible protein-membrane association, we set out to explore the capabilities of our approach on a relevant biomedical application. Anti-HIV broadly neutralizing Abs can neutralize genetically diverse HIV strains, usually targeting conserved regions of the Env protein close to the viral membrane. One peculiarity of most broadly neutralizing Abs, including 10E8 (21), is their functional association with the viral membrane: epitope binding and viral neutralization rely on Ab-lipid interactions (45,46). This has prompted the investigation of ways to improve Ab potency through engineering Ab-membrane interactions, stressing the relevance of quantitative understanding Ab-membrane partition mechanisms. 10E8-3R is an engineered anti-HIV1 broadly neutralizing Ab that attains increased potency through the enhancement of the electrostatic membrane interactions (22).

To investigate the partitional behavior of 10E8-3R onto the membrane, we performed FCS titration experiments using POPC:Chol:POPS membranes with varying concentrations of POPS and Chol. To this end, 10E8-3R was labeled with the fluorescent probe Abberior KK114 in its heavy chain. This position was chosen for its flexibility

Please cite this article in press as: Vesga et al., Quantitative characterization of membrane-protein reversible association using FCS, Biophysical Journal (2023), https://doi.org/10.1016/j.bpj.2023.01.026

and location away from the membrane, ensuring that the fluorophore would not perturb the partitional behavior onto the membrane. Fig. 6 *A* shows the effect of the different lipid compositions in 10E8-3R partitional behavior. Increasing Chol content in the membrane resulted in an almost proportional increase in Fab-membrane affinity ($K_x = 1.4 \times 10^5 \pm 0.5 \times 10^5$ for the 50:40:10 mixture, dotted blue line, and $K_x = 4.4 \times 10^4 \pm 0.3 \times 10^4$ for the 80:10:10 mixture, green dashed line). Maximal K_x enhancement was attained increasing the negatively charged lipid POPS ($K_x = 4.0 \times 10^5 \pm 0.1 \times 10^5$ for the 80:0:20 mixture, solid red line), highlighting the relevance of electrostatic interactions in 10E8-3R partition to the membrane (see also Fig. S2). Association to 100% POPC membranes was negligible or very low even at high lipid concentration, reflecting a substantially lower K_x than in the presence of either Chol or POPS (Fig. S2). Consistent with the CRB analysis (Fig. 5), K_x for POPC-only membranes could not be reliably determined since its value laid at the leftmost edge of the optimal interval for K_x determination. Interestingly f_{mem}^{sat} remained at around 0.70 irrespective of the content of Chol or POPS in the mixture for all Chol- or POPS-containing mixtures. f_{mem}^{sat} smaller than 1 indicates either the presence of free fluorescent dye in solution (13) or incomplete protein-membrane binding at large lipid concentrations, which has been previously ascribed to the presence of a protein conformer that is not membrane-competent (27). 10E8-3R fully associated to 80:0:20 vesicles that carried a small quantity of its antigen (Fig. S3), ruling out a significant effect of free dye or membrane-incompetent conformers and hinting, instead, at a rapid turnover of Fab on the vesicles as the underlying reason for the incomplete binding at large lipid concentrations.

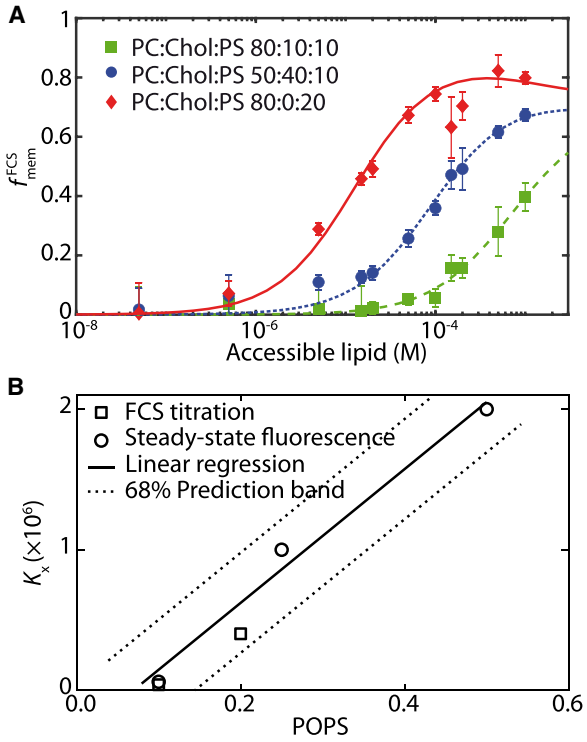

FIGURE 6 10E8-3R K_x determined by FCS titration. (*A*) 10E8-3R partition coefficient for POPC:Chol:POPS membranes with varying ratios of Chol and POPS. $K_x = 4.0 \times 10^5 \pm 0.1 \times 10^5$ for the 80:0:20 membrane (*diamonds*, *solid red line*); $K_x = 1.44 \times 10^5 \pm 0.05 \times 10^5$ for 50:40:10 (*circles*, *dotted blue line*) and $K_x = 4.43 \times 10^4 \pm 0.03 \times 10^4$ for 80:10:10 (*squares*, *dashed green line*). The graph shows that, even at maximal K_x (80:20:20), the titration curve does not reach 1, indicating the presence of Fab that remains in solution. In addition, f_{mem}^{sat} is very similar for all three compositions ($f_{mem}^{sat} = 0.69 \pm 0.02$ for the 80:0:20 membrane, 0.72 ± 0.02 for 50:40:10, and 0.72 ± 0.03 for 80:10:10). (*B*) K_x for 10E8-3R determined by FCS titration using a KK114-tagged 10E8-3R Fab on 90:0:10 and 80:0:20 membranes (*squares*) and by steady-state fluorescence spectroscopy exploiting the quantum-yield change upon membrane incorporation of an NBD-tagged 10E8-3R Fab (*circles*), previously reported in (22). The solid line is the linear regression of the K_x series determined by steady-state fluorescence spectroscopy (22), and the dotted line indicates the regression 68% prediction band. The K_x measured at 10% PS by both techniques overlap. The K_x determined at 20% PS by FCS titration falls within the 68% prediction band of previously reported K_x. This demonstrates that K_x determined by FCS titration are fully consistent with previous measurements using different techniques. The prediction band was calculated using SPA (41). To see this figure in color, go online.

Our results using FCS and a reversible association model are entirely consistent with previous studies on 10E8-3R partitional behavior (Fig. 6 *B*). 10E8-3R K_x for membranes that contain 10% and 20% POPS (squares) measured in this work (Fig. S2) follow the same trend observed for membranes containing 10%, 25%, and 50% POPS (circles), previously reported using 7-nitrobenz-2-oxa-1,3-diazol-4-yl (NBD) steady-state fluorescence spectroscopy (22). These results not only validate the use of FCS to determine K_x and the reversible association model but also confirm the validity of previous results on partitioning behavior using NBD.

DISCUSSION

In the present study, we have established the probability distribution of proteins reversibly associating to lipid vesicles and validated it using RD simulations. We have demonstrated the importance of considering the uneven distribution of protein on vesicles to quantify the lipid-membrane partition coefficient using FCS. We have also established the optimal range to determine K_x studying the CRB and performing computational FCS experiments. Finally, we have demonstrated the application of our work to the specific biological problem of antibody-membrane interactions.

Determination of K_x by fluorescence spectroscopy is advantageous since fluorescence-based methodologies are highly sensitive and do not require physical separation of the aqueous and lipid phases, resulting in a minimal perturbation of the system (9,10). In particular, FCS is especially well suited for K_x determination since, although some fluorescence-based methods rely on the use of probes that incorporate into the membrane and have a different quantum

Please cite this article in press as: Vesga et al., Quantitative characterization of membrane-protein reversible association using FCS, Biophysical Journal (2023), https://doi.org/10.1016/j.bpj.2023.01.026

yield in the aqueous phase and lipid phase, FCS has the advantage that the protein can be labeled at any residue located away from the protein-membrane interaction region, therefore reducing the risk of perturbing the protein partitional behavior.

Our work has established the probability distribution of proteins on vesicles for the case when proteins can spontaneously associate, dissociate, and reassociate to the membrane. There are many instances when the shape of the distribution of proteins on vesicles, and not only its average value, can be critical to the outcome of the experiment. We have shown that accurate quantification of K_x is one of these cases. Other relevant examples include the estimation of the number of Ab on virions (e.g., (47)), required to understand viral neutralization, and the design of drug delivery systems that make use of lipid vesicles or metallic nanoparticles when the biological molecule is adsorbed onto the vesicle membrane or the nanoparticle surface (e.g., (3) and references therein). We have shown that the way proteins distribute on lipid vesicles is markedly different when dissociation and reassociation events are considered compared with when dissociation is negligible. This is the case even when the probability of dissociation is very small (Fig. 3). Importantly, we have noticed that most scientific reports overlook the uneven distribution of protein on particles, or assume a Poisson distribution, which is only adequate when dissociation is negligible (Fig. 3 *D*). One of the reasons why this might be the case is that, both when the association is not reversible and when dissociation and reassociation events must be considered, the average number of proteins on vesicles, λ, is the same (Eq. 8). However, the shape of the distribution of proteins on vesicles is very different. When the association is not reversible, proteins are Poisson distributed on vesicles with a variance equal to λ. On the other hand, when dissociation and reassociation are considered, the pmf is given by Eq. 10 with a much larger variance equal to $\lambda(\lambda+1)$ (Eq. 11). Another consequence of the specific distribution of proteins on vesicles for reversible association is that the fraction of vesicles that do not carry any protein is not negligible (e.g., Fig. 3 *B* and *C*). This is in stark contrast to the case when the protein irreversibly binds to the vesicle, as, in the latter case, the distribution is Poissonian and the fraction of unloaded vesicles is much smaller and steeply decreases when λ increases (e.g., Fig. 3 *D*). Although we have focused on rigorous protein-membrane K_x quantification, the probability distribution derived in this work also describes the distribution of biomolecules adsorbed on a carrier particle when dissociation and reassociation are not negligible. In this regard, the wide spread of molecules on particles and the large number of unloaded particles may also have implications for biological and biotechnological applications that require quantification of the molecules carried by a particle.

Our work presents an extension and improvement of previous methodologies used to compute K_x using FCS (13,17,18). We introduce a new formalism to account for protein-membrane dissociation and reassociation events and formulate a probability distribution that describes the distribution of proteins on vesicles that undergo reversible association (Eq. 10). This allows the effects of the unequal distribution of protein on vesicles (11) and the different liposome brightness in the determination of bound protein fraction (13) to be rigorously considered. Reversible association with a highly dynamic turnover (determined by k_{off}) may also account for the frequent observation that the fraction of partitioned protein does not reach one asymptotically (Fig. 6 *A*), giving a different physical meaning to the f_{mem}^{sat} parameter in Eq. 4.

One straightforward simplification of the method occurs when the infinite protein dilution regime can be achieved. In this regime, the average number of protein copies per vesicle, λ, is $\lambda \leq 1$. In this case, almost all vesicles detected by FCS carry just one protein ($<q_2> = 1$) and thus the FCS fraction of partitioned protein, f_{mem}^{FCS}, is equal to the mole fraction, f_{mem} (Fig. 4 *B*). Another advantage of working at the infinite dilution regime is that both proteins and protein-loaded vesicles have the same brightness. This regime has already been addressed (17). However, on most occasions, the infinite dilution regime is not experimentally accessible due to the high concentration of lipid required to reach it. Therefore, the method described in this work is particularly suited to quantitatively describe protein-membrane association by titration when the infinite protein dilution regime is not experimentally attainable.

Labeling the lipid vesicles as well as the protein has recently been proved to be advantageous to retrieve K_x using FCCS (18) since the number of protein-loaded vesicles, n_2^F, in Eq. 21 can be directly estimated from the cross-correlation of the emission of the free protein and the vesicles. This way, information on the average number of protein copies per loaded vesicle $<q_2>$ can be obtained without the need to choose a specific statistical distribution of proteins on vesicles. In turn, this requires precise determination of the ACF value at time 0. Our method complements the information obtained by FCCS, since FCCS already provides the ACF for the tagged protein and its analysis using our approach comes at no additional experimental cost. In our work we have formulated the statistical distribution for non-stoichiometric binding. Using the statistical distribution matching the association problem under study provides information that is independent from the one obtained using cross-correlation, giving more profound insight into the protein-membrane binding mechanism.

CONCLUSIONS

In conclusion, we have established that FCS is a suitable technique for quantifying membrane-protein reversible association when the distribution of proteins on vesicles is

Please cite this article in press as: Vesga et al., Quantitative characterization of membrane-protein reversible association using FCS, Biophysical Journal (2023), https://doi.org/10.1016/j.bpj.2023.01.026

considered. Due to the random and non-homogeneous distribution of proteins on vesicles, the membrane-bound protein fraction observed by FCS carries information on both the membrane-bound protein mole fraction and the distribution of proteins on vesicles. We have derived the probability distribution of proteins on lipid vesicles when proteins can spontaneously associate, dissociate, and reassociate to the membrane and applied it to accurately determine K_x using FCS. The method presented in this work is particularly suitable for quantifying the affinity of functionally significant, although weak, interactions of proteins with membranes during many biology and physiology events, such as signaling or antigen recognition. Our work further extends the methodological spectrum of techniques available to study membrane-mediated biological events, allowing rigorous quantitative study of proteins that spontaneously dissociate and reassociate from and to the membrane.

SUPPORTING MATERIAL

Supporting material can be found online at https://doi.org/10.1016/j.bpj.2023.01.026.

AUTHOR CONTRIBUTIONS

J.R.I. designed the project, derived the theory for the probability distribution, and wrote the paper with comments from all authors. A.G.V. carried out the FCS bench experiments, designed and analyzed the computational FCS experiments, and performed the CRB study. L.V. designed the RDME simulations. C.C.V.S. designed the Brownian dynamics simulations. C.O.S.S. supervised the CRB analysis. A.G.V. and C.O.S.S. revised the paper. All authors read and approved the manuscript.

ACKNOWLEDGMENTS

This work was partially supported by Ministerio de Ciencia e Innovación (Spain) grant PID2021-125024NB-C21 funded by MCIN/AEI/10.13039/501100011033/FEDER, UE, and awarded to J.R.I. A.G.V. acknowledges funding from La Caixa Foundation ID 100010434 and LCF/BQ/DR19/11740034 and the Ministry of Education of Spain (FPU16/01727). We gratefully thank Prof. J.L. Nieva (University of the Basque Country, Spain) for kindly providing the labeled 10E8-3R Fab; J. Torralba, and M. Garcia-Porras for help with sample preparation; and Dr. P. Carravilla and Dr. L.A. Campos for critical discussion.

DECLARATION OF INTERESTS

The authors declare no competing interests.

SUPPORTING CITATIONS

References (48–56) appear in the Supporting material.

REFERENCES

1. Hollmann, A., M. Martinez, …, P. C. Maffia. 2018. Antimicrobial peptides: interaction with model and biological membranes and Synergism with chemical Antibiotics. *Front. Chem.* 6:204.
2. Ribeiro, M. M. B., M. N. Melo, …, M. A. R. B. Castanho. 2010. Drug-lipid interaction evaluation: why a 19th century solution? *Trends Pharmacol. Sci.* 31:449–454.
3. Nienhaus, K., Y. Xue, …, G. U. Nienhaus. 2022. Protein adsorption onto nanomaterials engineered for theranostic applications. *Nanotechnology.* 33:262001.
4. Carravilla, P., L. Darré, …, J. Requejo-Isidro. 2020. The bilayer collective properties govern the interaction of an HIV-1 antibody with the viral membrane. *Biophys. J.* 118:44–56.
5. Richens, J. L., J. S. Lane, …, P. O'Shea. 2015. The electrical interplay between proteins and lipids in membranes. *Biochim. Biophys. Acta.* 1848:1828–1836.
6. White, S. H., W. C. Wimley, …, K. Hristova. 1998. Protein folding in membranes: Determining energetics of peptide-bilayer interactions. *Methods Enzymol.* 295:62–87.
7. Yeagle, P. L. 2014. Non-covalent binding of membrane lipids to membrane proteins. *Biochim. Biophys. Acta.* 1838:1548–1559.
8. Mulgrew-Nesbitt, A., K. Diraviyam, …, D. Murray. 2006. The role of electrostatics in protein-membrane interactions. *Biochim. Biophys. Acta.* 1761:812–826.
9. Santos, N. C., M. Prieto, and M. A. R. B. Castanho. 2003. Quantifying molecular partition into model systems of biomembranes: an emphasis on optical spectroscopic methods. *Biochim. Biophys. Acta.* 1612:123–135.
10. Matos, P. M., H. G. Franquelim, …, N. C. Santos. 2010. Quantitative assessment of peptide-lipid interactions. Ubiquitous fluorescence methodologies. *Biochim. Biophys. Acta.* 1798:1999–2012.
11. Yu, L., M. Tan, …, T. Wohland. 2006. Determination of critical micelle concentrations and aggregation numbers by fluorescence correlation spectroscopy: Aggregation of a lipopolysaccharide. *Anal. Chim. Acta.* 556:216–225.
12. Kim, S. A., K. G. Heinze, …, P. Schwille. 2005. Two-photon cross-correlation analysis of intracellular reactions with variable stoichiometry. *Biophys. J.* 88:4319–4336.
13. Melo, A. M., M. Prieto, and A. Coutinho. 2011. The effect of variable liposome brightness on quantifying lipid-protein interactions using fluorescence correlation spectroscopy. *Biochim. Biophys. Acta.* 1808:2559–2568.
14. Ribeiro, M. M. B., M. N. Melo, …, M. A. R. B. Castanho. 2010. Drug-lipid interaction evaluation: why a 19th century solution? *Trends Pharmacol. Sci.* 31:449–454.
15. Elson, E. L. 2011. Fluorescence correlation spectroscopy: Past, present, future. *Biophys. J.* 101:2855–2870.
16. Thompson, N. L. 1991. Fluorescence correlation spectroscopy. *In* Topics in Fluorescence Spectroscopy, *Volume 1*. T. J. R. Lakowicz, ed. Plenum Press, pp. 337–378.
17. Rusu, L., A. Gambhir, …, J. Rädler. 2004. Fluorescence correlation spectroscopy studies of peptide and protein binding to phospholipid vesicles. *Biophys. J.* 87:1044–1053.
18. Krüger, D., J. Ebenhan, …, K. Bacia. 2017. Measuring protein binding to lipid vesicles by fluorescence cross-correlation spectroscopy. *Biophys. J.* 113:1311–1320.
19. Betaneli, V., J. Muecksch, and P. Schwille. 2019. Fluorescence correlation spectroscopy to examine protein-lipid interactions in membranes. *In* Methods in Molecular Biology. Lipid-Protein Interactions: Methods and Protocols, 2nd Edition. J. H. Kleinschmidt, ed, pp. 415–447.
20. Thomas, F. A., I. Visco, …, P. Schwille. 2015. Introducing a fluorescence-based standard to quantify protein partitioning into membranes. *Biochim. Biophys. Acta.* 1848:2932–2941.
21. Huang, J., G. Ofek, …, M. Connors. 2012. Broad and potent neutralization of HIV-1 by a gp41-specific human antibody. *Nature.* 491:406–412.
22. Rujas, E., D. P. Leaman, …, J. L. Nieva. 2018. Functional optimization of broadly neutralizing HIV-1 antibody 10E8 by promotion of membrane interactions. *J. Virol.* 92, e02249-17.

Please cite this article in press as: Vesga et al., Quantitative characterization of membrane-protein reversible association using FCS, Biophysical Journal (2023), https://doi.org/10.1016/j.bpj.2023.01.026

23. Kwon, Y. D., G.-Y. Chuang, …, P. D. Kwong. 2018. Surface-matrix screening identifies Semi-specific interactions that improve potency of a near Pan-reactive HIV-1-Neutralizing antibody. *Cell Rep.* 22:1798–1809.

24. Burton, D. R., and L. Hangartner. 2016. Broadly neutralizing antibodies to HIV and their role in vaccine design. *In* Annual Review of Immunology, *Vol 34* D. R. Littman and W. M. Yokoyama, eds., pp. 635–659.

25. Walker, L. M., and D. R. Burton. 2018. Passive immunotherapy of viral infections: 'super-antibodies' enter the fray. *Nat. Rev. Immunol.* 18:297–308.

26. Rhoades, E., T. F. Ramlall, …, D. Eliezer. 2006. Quantification of alpha-synuclein binding to lipid vesicles using fluorescence correlation spectroscopy. *Biophys. J.* 90:4692–4700.

27. Posokhov, Y. O., M. V. Rodnin, …, A. S. Ladokhin. 2008. Membrane insertion pathway of annexin B12: Thermodynamic and kinetic characterization by fluorescence correlation Spectroscopy and fluorescence quenching. *Biochemistry.* 47:5078–5087.

28. Gallea, J. I., E. E. Ambroggio, …, M. S. Celej. 2018. Amyloid oligomerization of the Parkinson's disease related protein alpha-synuclein impacts on its curvature-membrane sensitivity. *J. Neurochem.* 147:541–556.

29. Skellam, J. G. 1946. The frequency distribution of the difference between 2 poisson variates belonging to different populations. *J. R. Stat. Soc. Ser. A.* 109:296.

30. Gillespie, D. T. 1976. General method for numerically simulating stochastic time evolution of coupled chemical-reactions. *J. Comput. Phys.* 22:403–434.

31. Gibson, M. A., and J. Bruck. 2000. Efficient exact stochastic simulation of chemical systems with many species and many channels. *J. Phys. Chem. A.* 104:1876–1889.

32. Allen, M. P., and D. J. Tildesley. 2017. Computer Simulation of Liquids. Oxford University Press.

33. Frenkel, D., and B. Smit. 2002. Understanding Molecular Simulation: From Algorithms to Applications. Academic Press.

34. Elf, J., and M. Ehrenberg. 2004. Spontaneous separation of bi-stable biochemical systems into spatial domains of opposite phases. *Syst. Biol.* 1:230–236.

35. Hattne, J., D. Fange, and J. Elf. 2005. Stochastic reaction-diffusion simulation with MesoRD. *Bioinformatics.* 21:2923–2924.

36. Fange, D., and J. Elf. 2006. Noise-induced Min phenotypes in E-coli. *PLoS Comput. Biol.* 2:e80–e648.

37. Fange, D., O. G. Berg, …, J. Elf. 2010. Stochastic reaction-diffusion kinetics in the microscopic limit. *Proc. Natl. Acad. Sci. USA.* 107:19820–19825.

38. Dix, J. A., E. F. Y. Hom, and A. S. Verkman. 2006. Fluorescence correlation spectroscopy simulations of photophysical phenomena and molecular interactions: a molecular dynamics/Monte Carlo approach. *J. Phys. Chem. B.* 110:1896–1906.

39. Edholm, O., and J. F. Nagle. 2005. Areas of molecules in membranes consisting of mixtures. *Biophys. J.* 89:1827–1832.

40. Heras-Martínez, G. d. L., V. Calleja, …, J. Requejo-Isidro. 2019. A complex interplay of anionic phospholipid binding regulates 3′-phosphoinositide-dependent-kinase-1 homodimer activation. *Sci. Rep.* 9, 14527.

41. de las Heras-Martínez, G., J. Andrieu, …, J. Requejo-Isidro. 2018. Quantifying intracellular equilibrium dissociation constants using single-channel time-resolved FRET. *J. Biophotonics.* 11, e201600272.

42. Rujas, E., S. Insausti, …, J. M. M. Caaveiro. 2017. Functional Contacts between MPER and the anti-HIV-1 broadly neutralizing antibody 4E10 extend into the core of the membrane. *J. Mol. Biol.* 429:1213–1226.

43. Klein, J. S., P. N. P. Gnanapragasam, …, P. J. Bjorkman. 2009. Examination of the contributions of size and avidity to the neutralization mechanisms of the anti-HIV antibodies b12 and 4E10. *Proc. Natl. Acad. Sci. USA.* 106:7385–7390.

44. Luftig, M. A., M. Mattu, …, A. Carfí. 2006. Structural basis for HIV-1 neutralization by a gp41 fusion intermediate-directed antibody. *Nat. Struct. Mol. Biol.* 13:740–747.

45. Irimia, A., A. M. Serra, …, I. A. Wilson. 2017. Lipid interactions and angle of approach to the HIV-1 viral membrane of broadly neutralizing antibody 10E8: Insights for vaccine and therapeutic design. *PLoS Pathog.* 13:e1006212.

46. Rujas, E., J. M. M. Caaveiro, …, J. L. Nieva. 2016. Structural basis for broad neutralization of HIV-1 through the molecular recognition of 10E8 helical epitope at the membrane interface. *Sci. Rep.* 6:38177.

47. Klasse, P. J. 2007. Modeling how many envelope glycoprotein trimers per virion participate in human immunodeficiency virus infectivity and its neutralization by antibody. *Virology.* 369:245–262.

48. Kuramoto, Y. 1974. Effects of diffusion on fluctuations in open chemical systems. *Prog. Theor. Phys.* 52:711–713.

49. Gardiner, C. W., K. J. McNeil, …, I. S. Matheson. 1976. Correlations in stochastic theories of chemical-reactions. *J. Stat. Phys.* 14:307–331.

50. Baras, F., and M. M. Mansour. 1997. Microscopic simulations of chemical instabilities. *Adv. Chem. Phys.* D> 100:393–474.

51. Elf, J., A. Doncic, and M. Ehrenberg. 2003. Mesoscopic reaction-diffusion in intracellular signaling. *In* 1st International Symposium on Fluctuations and Noise, Santa Fe, Nm, pp. 114–124.

52. Bekker, H., H. J. C. Berendsen, …, M. K. R. Renardus. 1992. Gromacs - a parallel computer for molecular-dynamics simulations. *In* 4th International Conference on Computational Physics (PC 92), Prague, Czech Republic, pp. 252–256.

53. Pall, S., M. J. Abraham, …, E. Lindahl. 2014. Tackling exascale software challenges in molecular dynamics simulations with GROMACS. *In* 2nd International Conference on Exascale Applications and Software (EASC), Stockholm, SWEDEN, pp. 3–27.

54. Mandel, L. 1958. Fluctuations of photon beams and their correlations. *Proc. Phys. Soc.* 72:1037–1048.

55. Cramer, H. 1946. Mathematical Methods of Statistics. Princeton University Press.

56. Ries, J., M. Bayer, …, P. Schwille. 2010. Automated suppression of sample-related artifacts in fluorescence correlation spectroscopy. *Opt Express.* 18:11073–11082. https://www.osapublishing.org/viewmedia.cfm?uri=oe-11018-11011-11073&seq=11070&html=true.